JOURNAL OF PROPULSION AND POWER
Vol. 11, No. 3, May–June 1995

Inviscid Analysis of Transonic Oscillating Cascade Flows Using a Dynamic Mesh Algorithm

C. J. Hwang* and S. Y. Yang†
National Cheng Kung University, Tainan, Taiwan 701, Republic of China

A locally implicit total-variation-diminishing scheme and a rigid-deformable dynamic mesh algorithm are formulated on the quadrilateral-triangular meshes. The unsteady Euler equations with moving domain effects are solved in a Cartesian coordinate system. For transonic flows around an oscillating cascade of four biconvex blades with different oscillation amplitudes, reduced frequencies, and interblade phase angles, the calculated distributions of magnitude and phase angle of the first harmonic dynamic pressure difference coefficient agree better with experimental data than those from linearized theory and related numerical results on triangular meshes in most of the cases. Also, the numerical wiggles of instantaneous blade surface pressure coefficient distributions, which appeared on the triangular meshes, are eliminated. From the instantaneous pressure and Mach number contours, the unsteady flow phenomena, such as periodical characteristics, pressure wave and shock behaviors, and time-variations of zones with high Mach number gradient normal to the blade surfaces, are investigated. Furthermore, the lift coefficient distributions indicate that the oscillation amplitude, reduced frequency, and interblade phase angle all have significant effects on the transonic oscillating cascade flows.

Introduction

IN the development of turbomachines, one of the important concerns is blade vibration, which may cause structure failure. For solving two-dimensional oscillating cascade flows, the linearized models, such as the linearized potential[1] and Euler[2] solvers, have been used. Recently, a number of Euler solutions of the oscillating cascade flows were presented.[3–9] The numerical methods and periodical boundary treatments employed in those Euler solvers were briefly described in Ref. 9. As mentioned by Hwang and Yang,[9] further research on the Euler solution procedure for solving the oscillating cascade flows with nonlinear effects is still necessary and worthwhile. In this article, the locally implicit total-variation-diminishing (TVD) scheme on the dynamic triangular meshes,[9] is extended and formulated on the dynamic quadrilateral-triangular meshes. The simple spatial periodical boundary treatment,[9] which was proved to be more numerically stable than direct parameter storage method, is adopted.

In the calculations of oscillating cascade flows, several dynamic mesh algorithms on the quadrilaterals,[3,4,6,7] triangles,[8,9] and quadrilateral-triangular meshes[10] have been developed. To conform with the position of vibrating blades, Gerolymos[3] presented a grid displacement procedure, which permitted the simulation of large displacements. In order to save computing effort, a zonal moving grid treatment was developed by He.[4] Regarding this approach, only the grids in local regions around blades were moved, and the deformations of these cells were distributed to fit both the fixed region and the moving boundaries. On a mixed type of grids, where a deformable C-grid was used around blade surface and a H-grid was matched to the C-grid and extended as far upstream as necessary, Bendiksen[6] obtained the superior solution of the pressure. To fit with the moving blades, Huff[7] introduced a deforming grid technique to create C-grids. By stacking the C-grids for each blade, the multiple blade computational mesh was accomplished. Hsiao and Bendiksen[8] utilized the advancing front technique and conformal mapping procedure to generate a globally unstructured, but locally structured, blade-fitted deformable triangular-mesh system. Hwang and Yang[9] presented a dynamic triangular-mesh algorithm, where all the interior node positions in the computational domain were calculated and the deformable cells were in time to respond to the oscillating cascade of blades. Siden[10] created a dynamic quadrilateral-triangular mesh system. In this dynamic mesh, the structured quadrilateral meshes near the blade were deformed, while the outer triangular elements were kept fixed. From the grid distributions, the triangles and quadrilaterals on the interface of these two zones were overlapped. To save the computational efforts and maintain the quality of meshes, a rigid-deformable dynamic mesh algorithm is developed in this article. A layer of quadrilaterals around each blade surface is oscillated rigidly with respect to its own blade, and the triangles are distributed elsewhere and deformed in the same way as that of Ref. 9.

The purposes of this work are 1) to present a numerical solution approach for solving the unsteady Euler equations in the computational domain with complex geometries and moving boundaries, and 2) to investigate the unsteady flow phenomena and aerodynamic behaviors for transonic oscillating cascade flows with different oscillation amplitudes, interblade phase angles, and reduced frequencies. In the present numerical solution approach, extension of a locally implicit TVD scheme onto dynamic quadrilateral-triangular meshes, creation of a rigid-deformable dynamic mesh algorithm, quadrilateral-triangular mesh generation, spatially periodic boundary treatment, no-penetration condition on oscillating blade surfaces, and nonreflecting inlet/outlet boundary conditions are included. From the pressure coefficient distributions of the steady solutions for cascade of four biconvex blades, the present results are closer to the experimental data than those in Ref. 9. Furthermore, the instantaneous pressure coefficient distributions indicate that the use of quadrilateral-triangular meshes can eliminate the numerical wiggles appearing on the triangular meshes.[9] For the distributions of magnitude and phase angle of the first harmonic dynamic pressure difference coefficient, the present solutions show better agreement with the experimental data than those from linearized theory and Ref. 9 in most of the cases. From the instantaneous pressure

Received Sept. 25, 1993; presented as Paper 94-0146 at the AIAA 32nd Aerospace Sciences Meeting and Exhibit, Reno, NV, Jan. 10–13, 1994; revision received Aug. 8, 1994; accepted for publication Aug. 15, 1994.

*Professor, Institute of Aeronautics and Astronautics, 1 University Road. Member AIAA.

†Graduate Student, Institute of Aeronautics and Astronautics, 1 University Road.

and Mach number contours, the unsteady flow phenomena are investigated. According to the lift coefficient distributions, the effects of oscillation amplitude, interblade phase angle, and reduced frequency on the aerodynamic behaviors are further studied.

Numerical Solution Approach

In this work, the two-dimensional unsteady Euler equations including moving cell effects[11] are solved in the X-Y Cartesian coordinate system. Based on the numerical formulation presented in Ref. 11, the locally implicit TVD scheme[9] is extended and implemented on the dynamic quadrilateral-triangular meshes. Because this scheme incorporates an improved limiter function,[12] the unsteady shocks and pressure waves can be accurately resolved.

On the oscillating blade surface, the boundary treatment is the same as that applied on the oscillating airfoil surface in Ref. 11. A no-penetration boundary condition with respect to the moving surface is imposed. Pressure, density, and velocity component parallel to the oscillating blade surface are obtained by extrapolation from the values at the interior cells. On the periodic boundaries, a simple spatial treatment[9] is adopted. The same number of cells and nodes are generated along the upper and lower boundaries of the computational domain. The nodes on both boundaries are located at the same position along X-axis, but with a fixed distance in Y-axis, which is equal to the height of computational domain. Then, both the corresponding cells at upper and lower periodical boundaries are assigned to be the neighbors of each other, and they are treated like interior cells. At the inlet and outlet boundaries, a one-dimensional unsteady nonreflecting boundary condition, which was developed by Giles,[13] is utilized.

On the mixed mesh system (that is quadrilateral-triangular mesh system), a layer of O-typed quadrilaterals is generated around each blade surface to match the experimental geometry,[14] where the leading and trailing edges are rounded with a small radius of curvature. After creating the quadrilaterals, the unstructured triangles are distributed elsewhere according to the mesh generation algorithm.[15] Even though the dynamic mesh algorithm[9] can satisfactorily adjust the triangular cells to follow the motion of oscillating cascade blades, all the cells need to be processed for obtaining new grid positions during time evolution. To reduce the computational time and memory for calculating new grid positions, zonal dynamic grid techniques[4,10] were presented, where only the grids in local regions around oscillating blades were moved. The main problems of these approaches are 1) how many cells are sufficient to smoothly move the mesh and also maintain orthogonal to the blade surfaces in different oscillation situations and 2) how to accurately treat the zonal boundaries if grid points on the interface between two zones are not completely matched. In this article, a rigid-deformable dynamic mesh algorithm is developed. Instead of deforming the grids in the local regions around the blades, a layer of quadrilaterals around each blade surface is oscillated rigidly with respect to its own blade. The triangles, which are distributed elsewhere, are treated by the dynamic mesh algorithm.[9] The advantages of present rigid-deformable dynamic mesh algorithm over the globally deformable dynamic mesh algorithm[9] include 1) reducing computational time for calculating new grid positions during time evolution (in a flow computation of $\sigma = -90$ deg, $\alpha_1 = 1.2$ deg, and $k = 0.462$, it saves 48.6% CPU time for grid recalculations); and 2) maintaining the orthogonality on each blade surface (it's appropriate to simulate the boundary layer effects when viscous flows are studied in the future work). In the present rigid-deformable dynamic mesh algorithm, both of the quadrilateral (rigid) and triangular (deformable) dynamic meshes are treated as interior cells (i.e., single-block calculation). Therefore, there's no need to treat the interface boundary conditions.

Results and Discussion

In the present calculations of transonic oscillating cascade flows, the inlet Mach number and exit pressure ratio (static exit pressure divided by total pressure) are set to be 0.8 and 0.7322, respectively. The computational domain contains four uncambered biconvex blades, where the values of thickness-to-chord ratio, solidity (chord length divided by blade pitch), and stagger angle are 0.076, 1.3, and 53 deg, respectively. The motion of these four blades, which is executing torsional mode oscillations about midchord, is governed by the following relation

$$\alpha = \alpha_0 + \alpha_1 \sin(2Mk\tau + m\sigma) \tag{1}$$

where α, α_0, α_1, M, k, τ, and σ represent instantaneous angle of attack, mean flow angle of attack, oscillation amplitude, inlet Mach number, reduced frequency, nondimensionalized time scale, and interblade phase angle, respectively. The blade number $m = 0$, 1, 2, and 3 represent each blade from the lowest to the highest one, respectively. As shown in Fig. 1a, the mixed-mesh system contains 13,830 elements and 9619

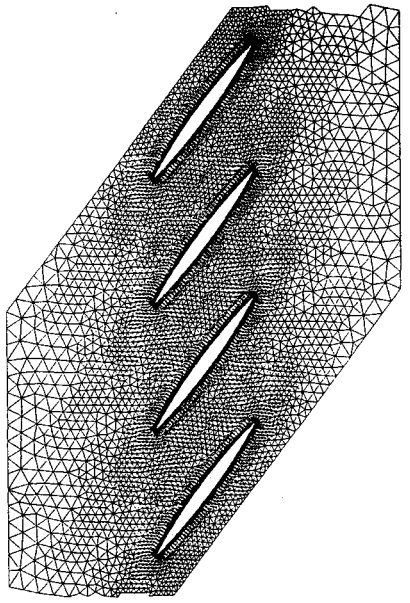

a)

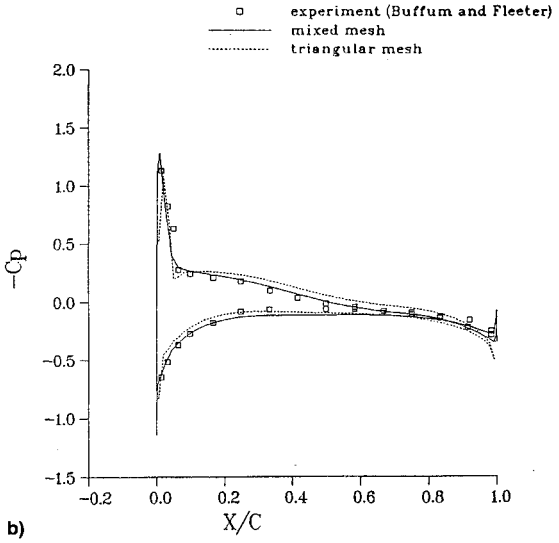

b)

Fig. 1 a) Partial view of quadrilateral-triangular meshes (13,830 elements and 9619 nodes) and b) pressure coefficient distributions of the initial solutions for an oscillating cascade of four biconvex blades.

nodes, where a layer of O-typed grids with 118 × 10 quadrilaterals is generated around each blade. By setting α_0 to be 7 deg, the pressure coefficient distributions of initial solutions (steady-state solutions) on purely triangular-[9] and mixed-mesh systems are plotted in Fig. 1b. For the triangular-mesh system, the leading and trailing edges of each blade are sharp, while those edges on mixed-mesh system are rounded with a small radius of curvature (0.33% of chord length) to match the experimental geometry.[14] As shown in Fig. 1b, the present numerical results on mixed meshes are closer to the experimental data[14] than those[9] on triangular meshes.

By choosing α_0 to be 7 deg, different oscillation amplitudes (α_I = 1.2, 2.4, 3.6, and 4.8 deg), reduced frequencies (k =

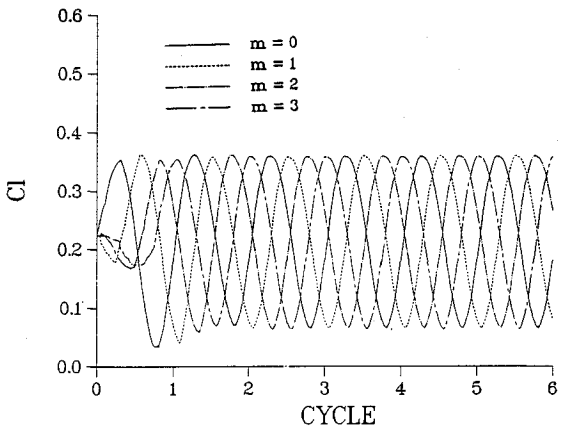

Fig. 2 Time history of lift coefficient for an oscillating cascade of four biconvex blades (M = 0.8, k = 0.462, α_0 = 7 deg, α_I = 1.2 deg, and σ = −90 deg).

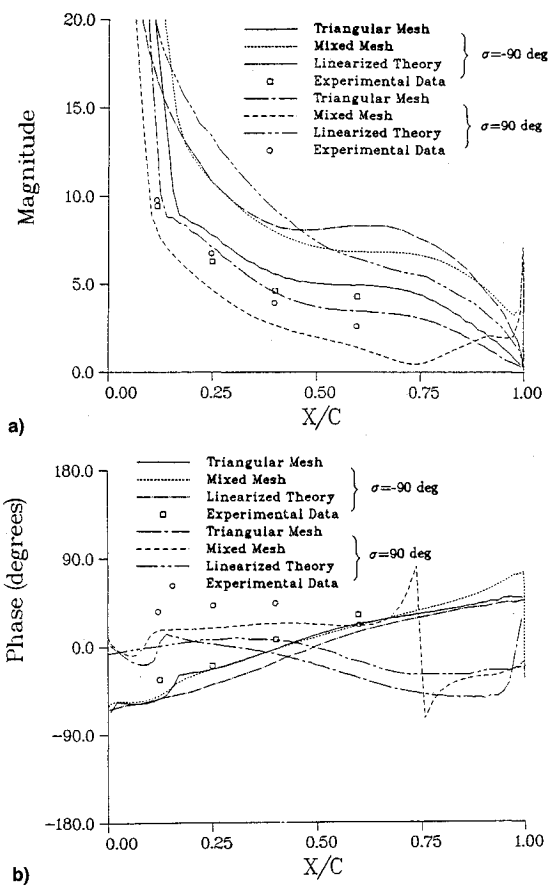

Fig. 3 a) Magnitude and b) phase angle of the first harmonic dynamic pressure difference coefficient ΔC_p for an oscillating cascade of four biconvex blades (M = 0.8, k = 0.185, α_0 = 7 deg, and α_I = 1.2 deg).

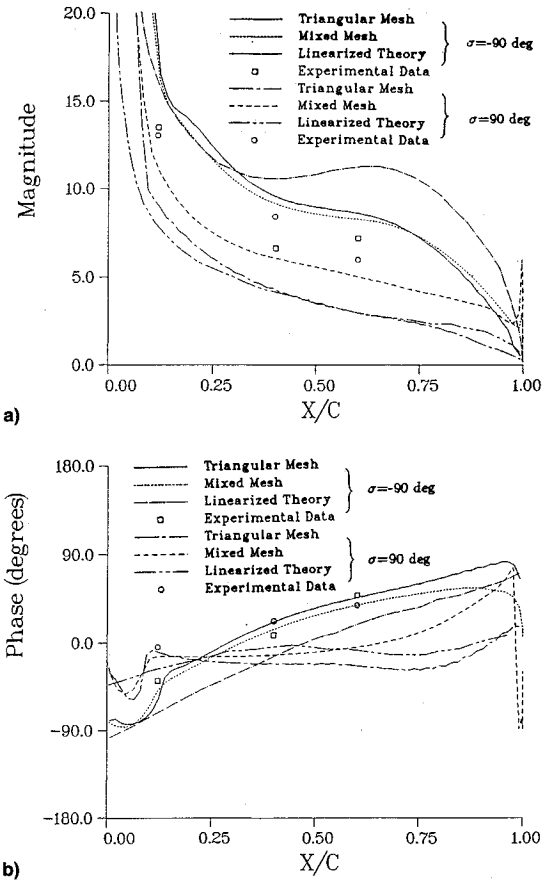

Fig. 4 a) Magnitude and b) phase angle of the first harmonic dynamic pressure difference coefficient ΔC_p for an oscillating cascade of four biconvex blades (M = 0.8, k = 0.462, α_0 = 7 deg, and α_I = 1.2 deg).

0.462 and 0.185), and interblade phase angles (σ = 90 and −90 deg) are employed in the present calculations. To consider the first cycle of blade motion for σ equal to −90 deg, only the lowest blade (m = 0) is set to motion at the beginning, whereas the second (m = 1), the third (m = 2), and the highest (m = 3) blades are set to motion when $2Mk\tau$ reaches $\pi/2$, π, and $3\pi/2$, respectively. As for σ replaced by 90 deg, the lowest blade (m = 0) is still set to motion at the beginning of the first cycle of motion, whereas the highest (m = 3), the third (m = 2), and the second (m = 1) blades are set to motion when $2Mk\tau$ reaches $\pi/2$, π, and $3\pi/2$, respectively. Once the blade is set to motion, it will continue its motion until the end of computation. For transonic oscillating cascade flows with σ, k, and α_I equal to −90 deg, 0.462, and 1.2 deg, respectively, a constant marching time step of $\Delta\tau$ = 0.0079 is chosen, and the periodic solution is achieved by processing six cycles of motion. In this computation, the maximum value of CFL is about 23, and it takes 1080 time steps (around 6.28 CPU hours) to accomplish one cycle of motion on the HP-720 workstation. From the time history of lift coefficient shown in Fig. 2, the periodic solution is quickly achieved, so that the present solution approach is efficient.

When one value of α_I (1.2 deg) and two values of σ (90 and −90 deg) are employed, magnitudes and phase angles of the first harmonic dynamic surface pressure difference coefficient ΔC_p are calculated and plotted in Fig. 3 (k = 0.185) and Fig. 4 (k = 0.462). As shown in those figures, the Euler solutions[9] on a triangular-mesh system, experimental data,[14] and numerical results[14] obtained by linearized theory are adopted for comparison. The results of linearized theory, which were predicted from the unsteady, small perturbation, subsonic, flat plate cascade analyses of Refs. 16 and 17, were directly extracted from the paper presented by Buffum and

Fleeter.[14] By choosing the experimental data as the reference values, the Euler solvers on triangular- and mixed-mesh systems (Fig. 3a) provide the better distributions of magnitude than does the linearized theory. Also, the Euler results obtained on triangular-mesh system are closer to the experimental data. From the phase angle distributions with σ equal to -90 deg (Fig. 3b), the numerical results on both mesh systems agree better with the experimental data than those by the linearized theory. Except the rear portion of the blade, the distributions of phase angle obtained on both mesh systems are close to each other. If the value of σ is replaced by 90 deg, the differences between experimental data and three numerical results are significant, whereas the present solution is closest to the data of experiment (Fig. 3b). Based on the discussion in Ref. 18, which was presented to explain the jump behavior at the trailing edge for the oscillating flat plate cascade, the phase discontinuity at 75% chord in Fig. 3b is a result of the corresponding magnitude (Fig. 3a) approaching zero, thereby making any slight difference become large. As for the magnitude distributions with $k = 0.462$ (Fig. 4a), especially for the case with σ equal to 90 deg, the present calculations on a mixed-mesh system demonstrate the best agreement with experimental data among three numerical results. From the distributions of phase angle ($\sigma = -90$ deg, Fig. 4b), the numerical solutions on triangular- and mixed-mesh systems are closer to the experimental data than those by linearized theory. Considering the case with σ replaced by 90 deg, the values of phase angle from linearized theory and both Euler calculations deviate a distance from experimental data. For both Euler calculations, this distance becomes smaller if a mixed-mesh system is utilized. According to the formula provided by Buffum and Fleeter,[19] Hwang and Yang[9] indicated that the calculation ($k = 0.462$, $\sigma = 90$ deg, and $\alpha_I = 1.2$ deg) lay within the super-resonant region. In super-resonant flow, the pressure waves will propagate upstream and downstream to infinity without decay, which may account for some of the discrepancies.[9] From the aforementioned discussion, the present solution approach is reliable and suitable for investigating the inviscid transonic oscillating cascade flows.

Considering the case with k, σ, and α_I equal to 0.462, -90 deg, and 1.2 deg, respectively, the instantaneous pressure contours on the mixed-mesh system during the sixth cycle [$(2Mk\tau - 10\pi) = \pi/2$, π, $3\pi/2$, and 2π] are plotted in Figs. 5a–5d. From those contours, it is observed that the flow behaviors repeat and proceed one pitch distance in the upward direction for each quarter-time period. As shown in Fig. 5a, a shock on the front part of upper surface of the highest blade ($m = 3$), a weak shock on the front part of upper surface of

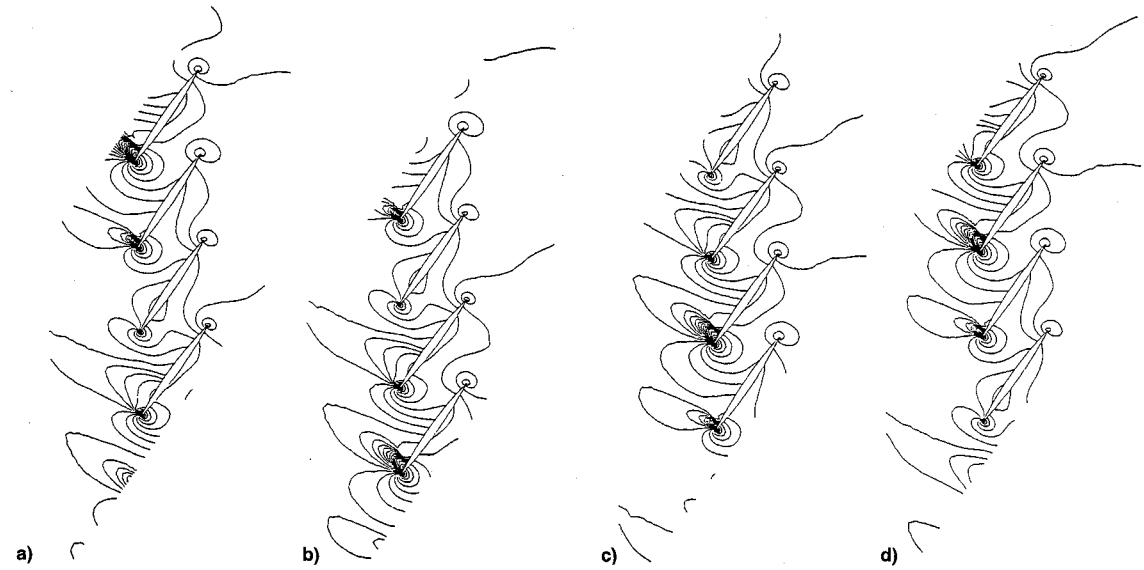

Fig. 5 Instantaneous pressure contours for an oscillating cascade of four biconvex blades ($M = 0.8$, $k = 0.462$, $\alpha_0 = 7$ deg, $\alpha_I = 1.2$ deg, and $\sigma = -90$ deg): ($2Mk\tau - 10\pi$) equal to a) $\pi/2$, b) π, c) $3\pi/2$, and d) 2π.

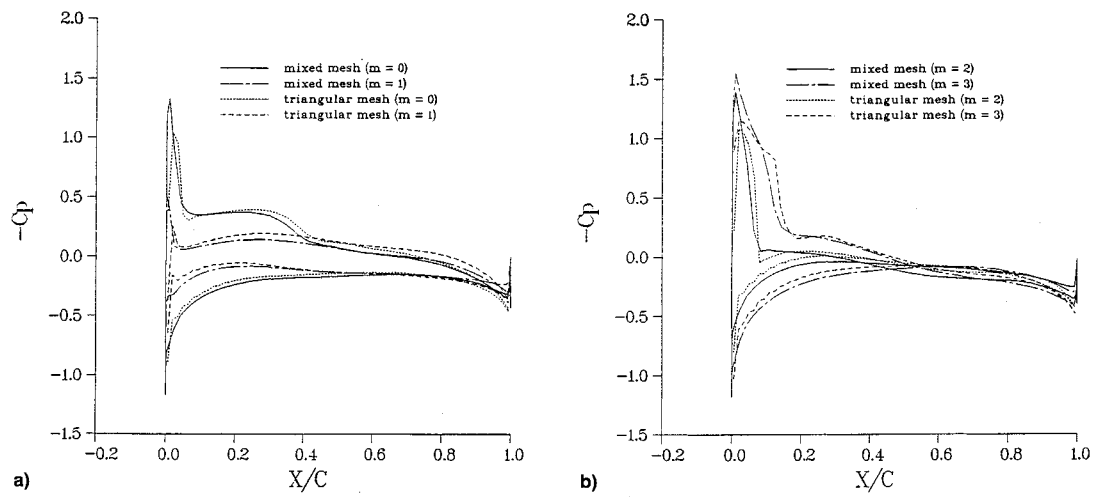

Fig. 6 Instantaneous blade surface pressure coefficient distributions for an oscillating cascade of four biconvex blades [$M = 0.8$, $k = 0.462$, $\alpha_0 = 7$ deg, $\alpha_I = 1.2$ deg, $\sigma = -90$ deg, and ($2Mk\tau - 10\pi$) = $\pi/2$]: a) the lowest and the second blades and b) the third and the highest blades.

the third blade ($m = 2$), and a weaker leading-edge shock on the upper surface of the lowest blade ($m = 0$) are observed. From the instantaneous blade surface pressure coefficient distributions at $(2Mk\tau - 10\pi) = \pi/2$ (Fig. 6), the positions and strength of shocks on the front parts of upper surfaces of the lowest ($m = 0$), third ($m = 2$), and highest ($m = 3$) blades are different for triangular- and mixed-mesh systems. Also, the wiggles of instantaneous pressure coefficient distributions on the front parts of lower surfaces of the blades, which are observed on triangular-mesh system, can be avoided if the mixed-mesh system is used.

To understand the effect of oscillation amplitude on the unsteady flow phenomena, α_I is amplified to 4.8 deg, whereas σ and k are set to be -90 deg and 0.462. From the instantaneous pressure contours (Figs. 7a–7d), it is apparent that the flow behaviors repeat and proceed one pitch distance in the upward direction for each quarter-time period. Compared with the contour given in Fig. 5a ($\alpha_I = 1.2$ deg), the shocks on the front parts of upper surfaces of the third and highest blades become stronger and move downstream, and the compression wave located near the midchord of upper surface of the highest blade merges together. At the same time, the compression wave near the midchord of upper surface of the lowest blade grows to be a shock, and an additional shock on the front part of lower surface of the second blade comes into view. Also, the weak leading shock on the upper surface of the lowest blade weakens itself to be a compression wave.

When σ is replaced by 90 deg while α_I and k are set to be 4.8 deg and 0.462, respectively, the instantaneous pressure and Mach number contours (Figs. 8 and 9) are plotted to study the effects of interblade phase angle on the unsteady flow phenomena. It is obvious that the flow phenomena repeat and proceed one pitch distance in the downward direction for every quarter-time period. From the results given in Figs. 8a and 9a, shocks appear on the front part of the upper surface of the lowest blade, and on the midchord of upper surface of the second blade. Also, the compression waves on the rear part of the lower surface of the third blade, and on the front

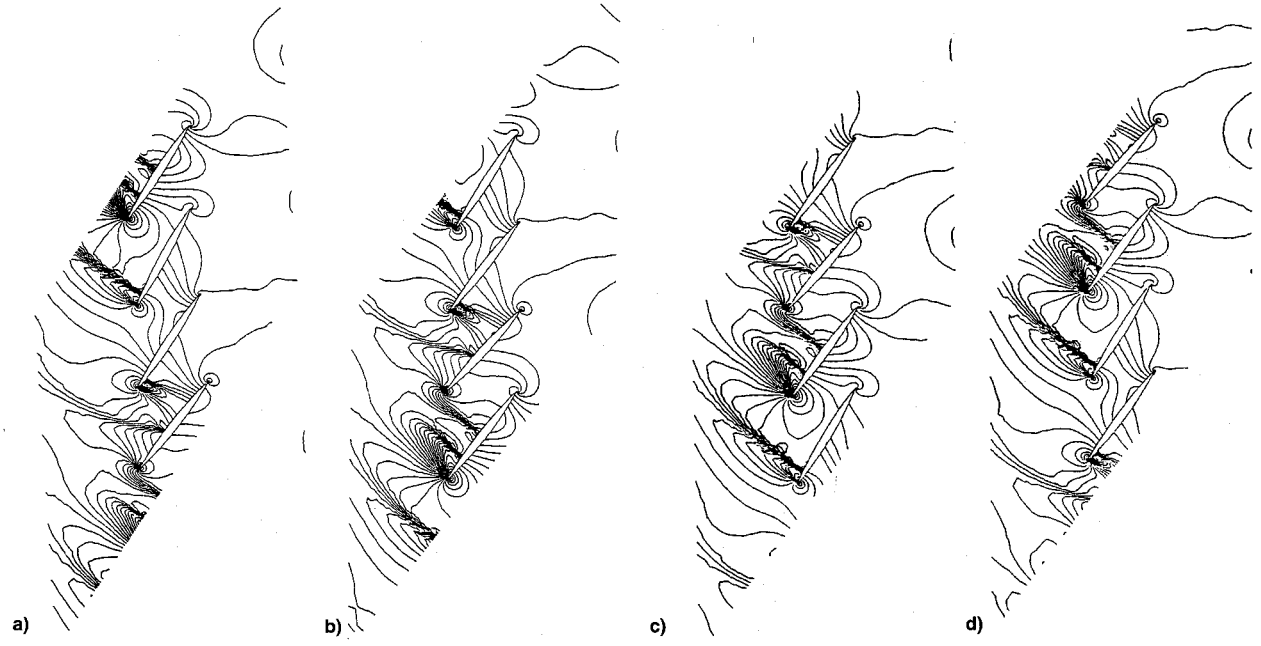

Fig. 7 Instantaneous pressure contours for an oscillating cascade of four biconvex blades ($M = 0.8$, $k = 0.462$, $\alpha_0 = 7$ deg, $\alpha_I = 4.8$ deg, and $\sigma = -90$ deg): $(2Mk\tau - 10\pi)$ equal to a) $\pi/2$, b) π, c) $3\pi/2$, and d) 2π.

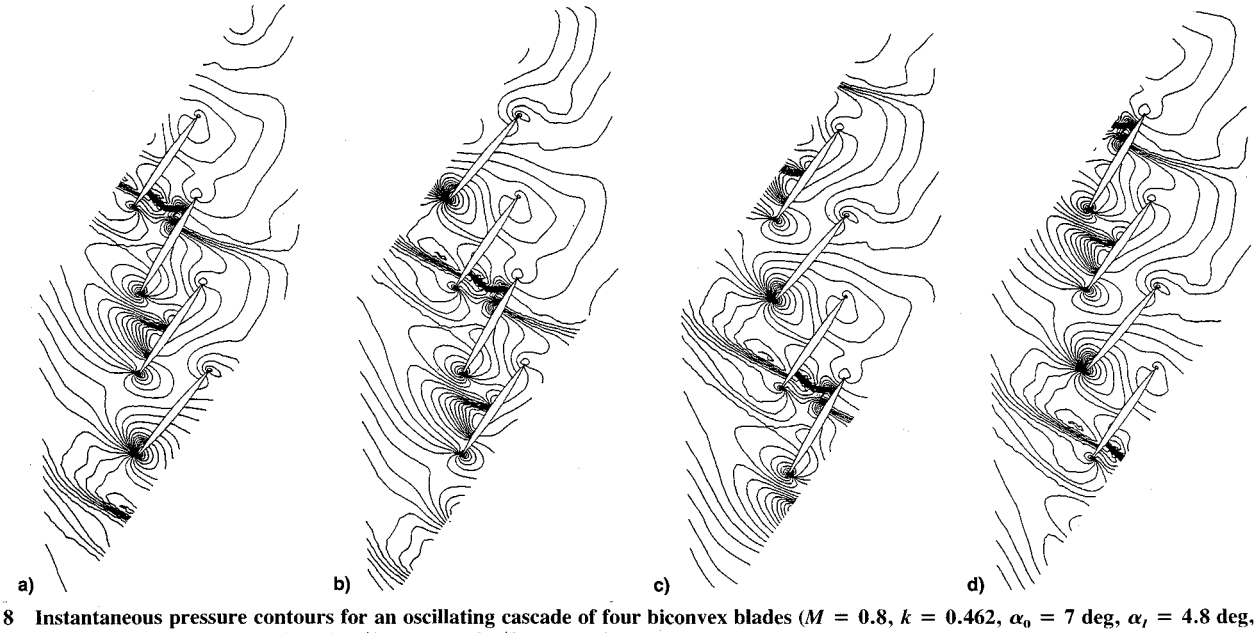

Fig. 8 Instantaneous pressure contours for an oscillating cascade of four biconvex blades ($M = 0.8$, $k = 0.462$, $\alpha_0 = 7$ deg, $\alpha_I = 4.8$ deg, and $\sigma = 90$ deg): $(2Mk\tau - 10\pi)$ equal to a) $\pi/2$, b) π, c) $3\pi/2$, and d) 2π.

part of upper surface of the highest blade are observed. Within the passage between the highest and third blades, a strong shock wave is depicted, whose strength is strong enough to choke the flow within that passage. According to the above discussion and the contours shown in Figs. 7a–7d ($\sigma = -90$ deg), completely different unsteady phenomena are observed. The effects of σ on the pressure contours are clearly indicated. From the Mach number contour given in Fig. 9a, zones with a high Mach number normal gradient appear on the upper surfaces of the lowest and the second blades, the rear part of the upper surface of the third blade, and the lower surface of the highest blade. Because the pressure and density on the blade surface are the same as those at the interior cell, which is nearest to the blade, the normal gradient of Mach number on the blade surface is decided by the gradient of velocity magnitude in the direction normal to the blade. In other words, the normal gradient of velocity magnitude in the zone with a high Mach number gradient on the blade surface is large. This phenomenon, which was not observed on the triangular-mesh system,[9] may be due to rounded trailing and leading edges of the blades when the mixed-mesh system is used.

Due to the periodic characteristics, the pressure contour in Fig. 8d and Mach number contour in Fig. 9d are the same as the corresponding contours at $2Mk\tau$ equal to 10π. The sequence of instantaneous pressure and Mach number contours at $(2Mk\tau - 10\pi) = 2\pi$ (Figs. 8d and 9d), $\pi/12$, $\pi/6$, $\pi/4$, $\pi/3$ (Figs. 10 and 11), and $\pi/2$ (Figs. 8a and 9a) are introduced to further investigate the unsteady behaviors during each quarter-time period. As shown in Figs. 8d and 9d, a compression wave appears on the front portion of the upper surface of the lowest blade, and a shock, which stands on the front part of the lower surface of the lowest blade and the rear part of the upper surface of the highest blade, chokes the flow within that passage. During time marching, both of the shock and compression waves move upstream, and the shock becomes a strong compression wave (Figs. 10a and 11a). At this moment, the flow within the above-mentioned passage is unchoked. This strong compression wave passes through the leading edge and combines with the upper compression wave (Figs. 10b and 11b). Then this compression wave continues to go upstream and decreases its strength (Figs. 8a and 9a). In the same time, a weak shock is formed on the front part

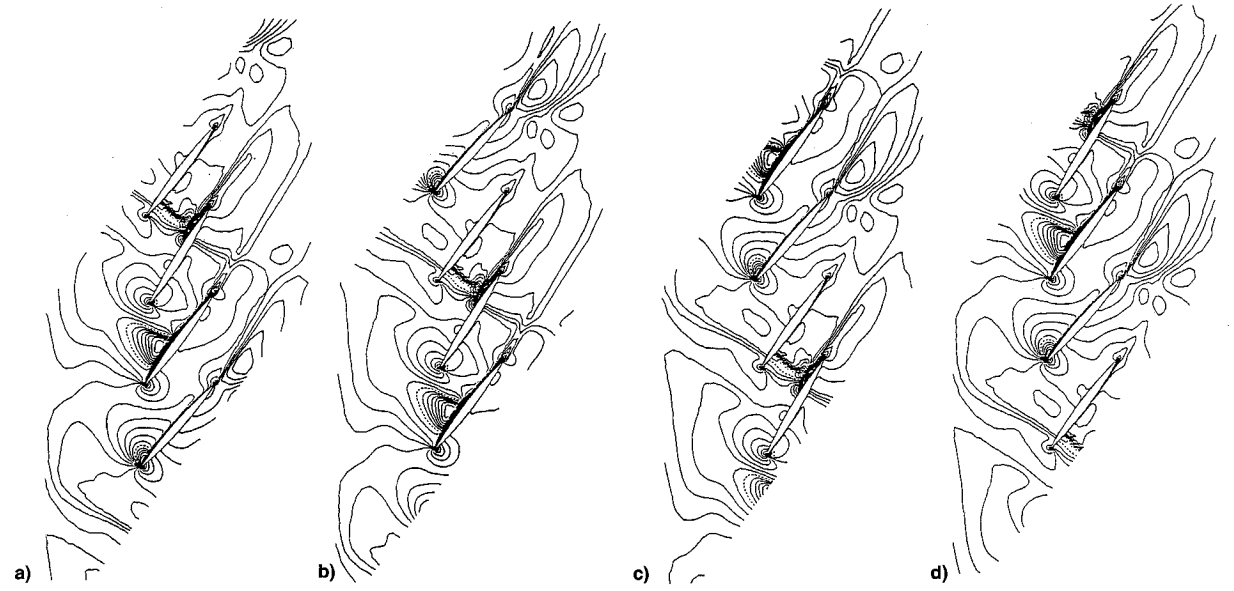

Fig. 9 Instantaneous Mach number contours for an oscillating cascade of four biconvex blades ($M = 0.8$, $k = 0.462$, $\alpha_0 = 7$ deg, $\alpha_I = 4.8$ deg, and $\sigma = 90$ deg): ($2Mk\tau - 10\pi$) equal to a) $\pi/2$, b) π, c) $3\pi/2$, and d) 2π.

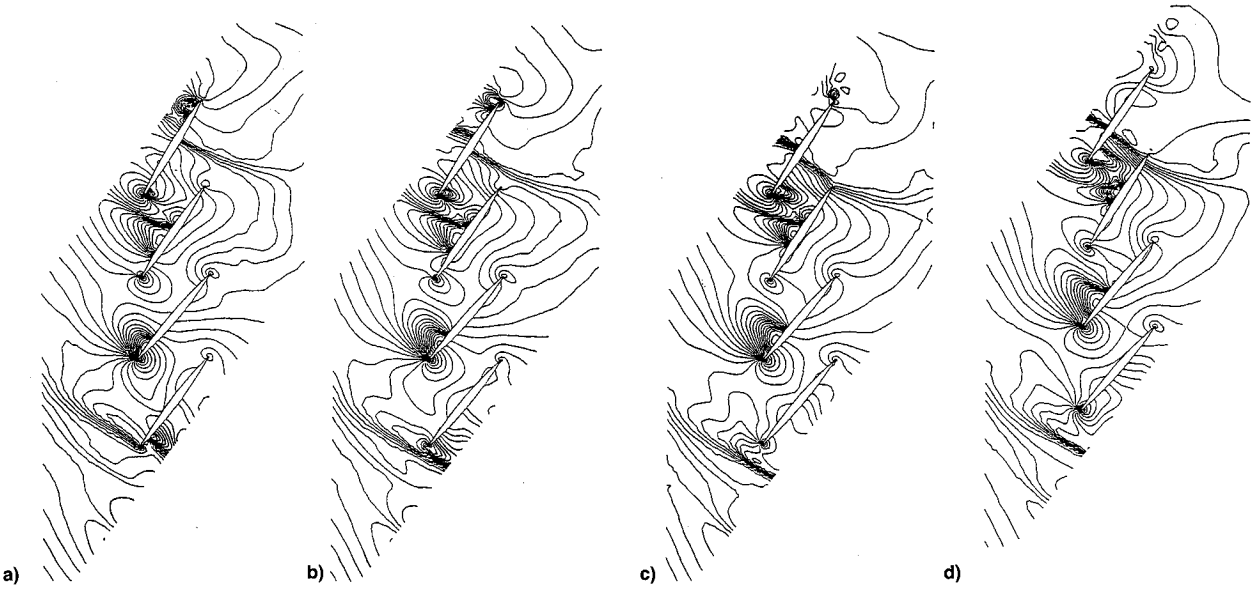

Fig. 10 Instantaneous pressure contours for an oscillating cascade of four biconvex blades ($M = 0.8$, $k = 0.462$, $\alpha_0 = 7$ deg, $\alpha_I = 4.8$ deg, and $\sigma = 90$ deg): ($2Mk\tau - 10\pi$) equal to a) $\pi/12$, b) $\pi/6$, c) $\pi/4$, and d) $\pi/3$.

of upper surface of the lowest blade (Figs. 8a and 9a). From the sequence of contours, a weak shock, which originally appears near the leading edge of the upper surface of the second blade (Figs 8d and 9d), moves downstream and becomes stronger. In the meantime, the compression wave on the rear part of lower surface of the highest blade (Figs. 8d and 9d) moves upstream. After passing through the trailing edge of the third blade, this compression wave is divided into two parts, and are located on the upper and lower surfaces of the third blade, respectively (Figs. 10c and 11c). Then both compression waves keep going upstream. On the other hand, a weaker leading-edge shock on the lower surface of the highest blade grows to be stronger and moves downstream. After interaction with the shock standing near the midchord of the upper surface of the third blade, a stronger shock is formed (Figs. 10d and 11d). At this moment, the flow within the passage between the highest and third blades is choked by this shock. Then this shock combines with the upper compression wave, which was cut by the trailing edge of the third blade, and becomes stronger (Figs. 8a and 9a). From the sequence of Mach number contours shown in Figs. 9d, 11a–11d, and 9a, the zone with a high normal gradient of Mach

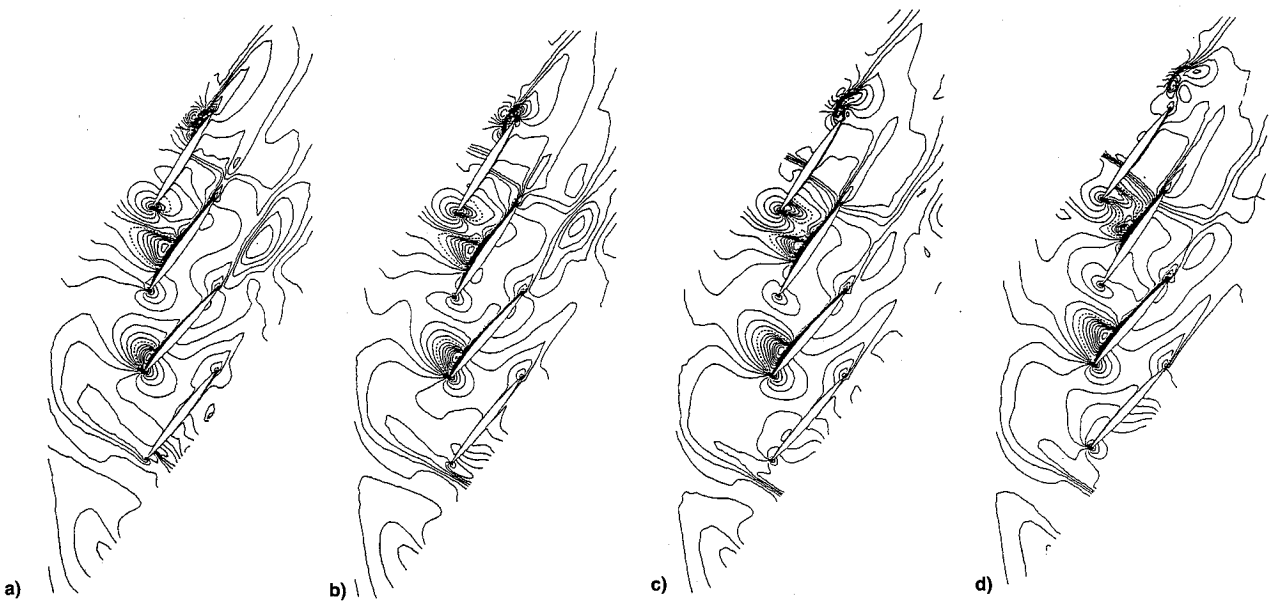

Fig. 11 Instantaneous Mach number contours for an oscillating cascade of four biconvex blades ($M = 0.8$, $k = 0.462$, $\alpha_0 = 7$ deg, $\alpha_I = 4.8$ deg, and $\sigma = 90$ deg): ($2Mk\tau - 10\pi$) equal to a) $\pi/12$, b) $\pi/6$, c) $\pi/4$, and d) $\pi/3$.

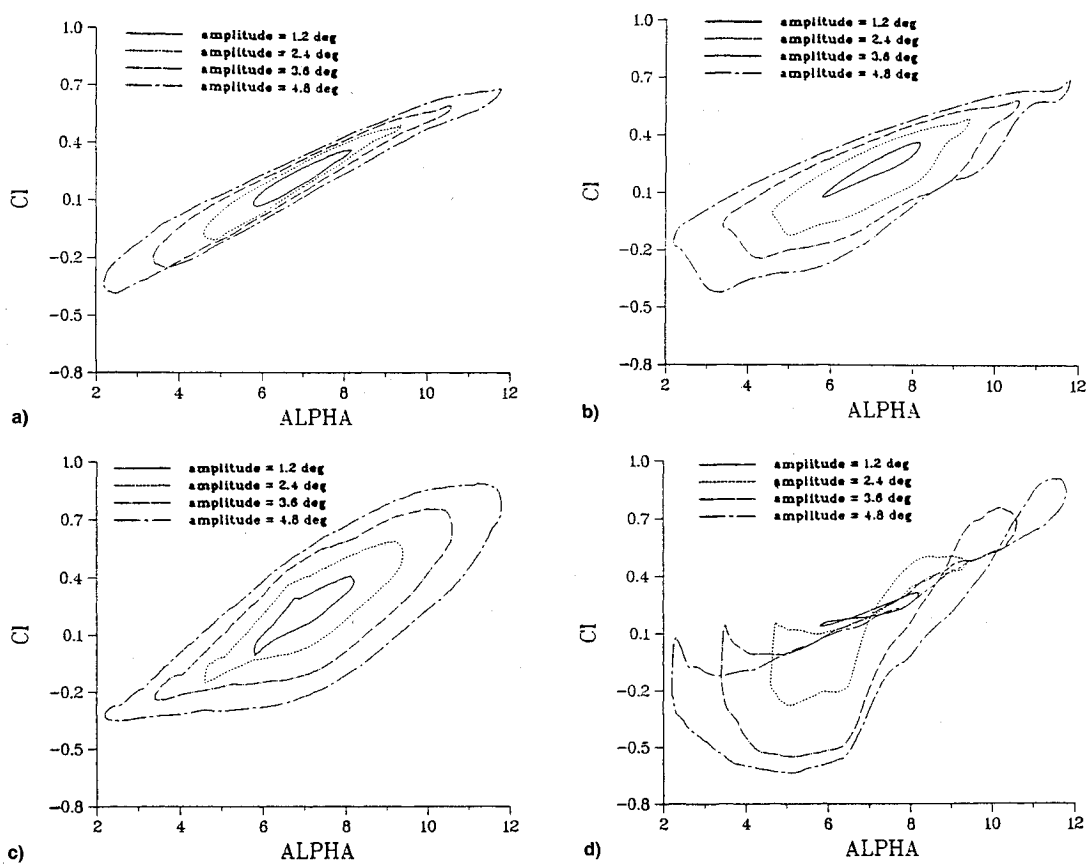

Fig. 12 Lift coefficient vs instantaneous angle of attack for the lowest blade of an oscillating cascade of four biconvex blades: a) $k = 0.462$, $\sigma = -90$ deg; b) $k = 0.462$, $\sigma = 90$ deg; c) $k = 0.185$, $\sigma = -90$ deg; and d) $k = 0.185$, $\sigma = 90$ deg.

number on the lower surface of the lowest blade (Fig. 9d) becomes thinner and eventually goes out of sight, whereas a new zone appears on the upper surface of the lowest blade (Fig. 9a). On the upper surface of the second blade, the zone with high normal gradient of Mach number keeps growing thicker. On the upper surface of the third blade, the front part of the zone with a high Mach number normal gradient dies out gradually, whereas the rear part of this zone grows thicker. Meanwhile, the zone on the rear part of the upper surface of the highest blade moves downstream and finally disappears. Besides the aforementioned time-variations of the zones with a high Mach number normal gradient, a thin zone on the lower surface of the highest blade shifts from the front portion to the rear region.

After the above-mentioned unsteady flow phenomena are predicted, it is important to study the unsteady aerodynamics. The lift coefficients on the lowest blade during the sixth cycle are calculated and plotted in Fig. 12 for the different values of k, σ, and α_f. At any instant positions (except the highest and lowest ones) of the lowest blade, the value of C_l for the blade moving upward is smaller than that for the blade moving downward (Figs. 12a–12c). Furthermore, the smallest C_l occurs a little late after the blade passes through it's lowest position for most of the cases in Figs. 12a–12c, and the largest C_l happens a little late after the blade passes it's highest position (Fig. 12c). In the present calculations with k and σ equal to 0.185 and 90 deg, respectively, the aerodynamic behaviors (Fig. 12d) are different from those in Figs. 12a–12c. When the blade moves upward, the values of C_l at some positions are higher than those for the blade moving downward. At a particular angle of attack, whose value is dependent on the amplitude of oscillation, both values of C_L for the blade moving upward and downward are identical to each other. Also, the smallest C_L occurs very late after the blade passes through its lowest position. When the value of σ is equal to 90 deg, especially for the case with $k = 0.185$, the present distributions of lift coefficient are significantly different from those[9] on the triangular-mesh system. From the aforementioned unsteady phenomena, it is believed that this big difference is due to the interaction between the compression wave and trailing edge of the blade. In this work, the round edge is employed, but the trailing edge was sharp when the triangular-mesh system was used. Based on the results shown in Fig. 12, the oscillation amplitude, interblade phase angle, and reduced frequency all have significant effects on aerodynamic behaviors.

Conclusions

A locally implicit algorithm with an improved limiter function on dynamic quadrilateral-triangular meshes is presented and utilized to investigate transonic flows around an oscillating cascade of four biconvex blades. The unsteady Euler equations are solved in a Cartesian coordinate system. On the quadrilateral-triangular mesh system, the leading and trailing edges are rounded with a small radius of curvature to match experimental geometry. A layer of O-typed quadrilaterals is generated around each blade, and the unstructured triangles are created elsewhere. To maintain the orthogonality on blade surfaces and reduce the computational efforts, a rigid-deformable dynamic mesh algorithm, where the layer of quadrilaterals is oscillated rigidly with respect to its own blade and the triangles are deformed by the previously developed dynamic mesh algorithm,[9] is presented in this article. From the pressure coefficient distributions of initial solutions, the present result on a quadrilateral-triangular mesh system agrees better with the experimental data than the related numerical result on a triangular-mesh system. For the distributions of magnitude and phase angle of the first harmonic dynamic pressure difference coefficient, the present solutions show better agreement with experimental data than those from linearized theory and related numerical results on a triangular-mesh system in most of the cases. Also, the numerical wiggles of the instantaneous blade surface pressure coefficient distributions appearing on the triangular-mesh system are eliminated. At every quarter-time period, the pressure and/or Mach number contours repeat and proceed one pitch distance in the upward or downward direction for an interblade phase angle equal to -90 or 90 deg, respectively. The unsteady flow phenomena, such as shock formation, migration, strengthening, attenuation, interaction with pressure wave, and time-variations of zones with high Mach number normal gradient along the blade surfaces, are observed. From the lift coefficient distributions and instantaneous pressure contours, the oscillation amplitude, reduced frequency, and interblade phase angle all significantly affect the unsteady phenomena and aerodynamic behaviors of transonic oscillating cascade flows.

References

[1]Usab, W. J., Jr., and Verdon, J. M., "Advances in the Numerical Analysis of Linearized Unsteady Cascade Flows," *Journal of Turbomachinery*, Vol. 113, No. 4, 1991, pp. 633–643.

[2]Hall, K. C., and Crawley, E. F., "Calculation of Unsteady Flows in Turbomachinery Using the Linearized Euler Equations," *AIAA Journal*, Vol. 27, No. 6, 1989, pp. 777–787.

[3]Gerolymos, G. A., "Numerical Integration of the Blade-to-Blade Surface Euler Equations in Vibrating Cascades," *AIAA Journal*, Vol. 26, No. 12, 1988, pp. 1483–1492.

[4]He, L., "An Euler Solution for Unsteady Flows Around Oscillating Blades," *Journal of Turbomachinery*, Vol. 112, No. 4, 1990, pp. 714–722.

[5]Huff, D. L., Swafford, T. W., and Reddy, T. S. R., "Euler Flow Predictions for an Oscillating Cascade Using a High Resolution Wave-Split Scheme," American Society of Mechanical Engineers Paper 91-GT-198, June 1991.

[6]Bendiksen, O. O., "Euler Calculations of Unsteady Transonic Flow in Cascades," AIAA Paper 91-1104, April 1991.

[7]Huff, D. L., "Numerical Analysis of Flow Through Oscillating Cascade Sections," *Journal of Propulsion and Power*, Vol. 8, No. 4, 1992, pp. 815–822.

[8]Hsiao, C., and Bendiksen, O. O., "Finite Element Euler Calculations of Unsteady Transonic Cascade Flows," *Proceedings of the Dynamics Specialist Conference*, 1992, pp. 389–400 (AIAA Paper 92-2120).

[9]Hwang, C. J., and Yang, S. Y., "Euler Solutions for Transonic Oscillating Cascade Flows Using Dynamic Triangular Meshes," American Society of Mechanical Engineers Paper 93-GT-93, May 1993.

[10]Siden, L. D. G., "Numerical Simulation of Unsteady Viscous Compressible Flows Applied to Blade Flutter Analysis," American Society of Mechanical Engineers Paper 91-GT-203, June 1991.

[11]Hwang, C. J., and Yang, S. Y., "Locally Implicit Total-Variation-Diminishing Schemes on Mixed Quadrilateral-Triangular Meshes," *AIAA Journal*, Vol. 31, No. 11, 1993, pp. 2008–2015.

[12]Hwang, C. J., and Liu, J. L., "Locally Implicit Hybrid Algorithm for Steady and Unsteady Viscous Flows," *AIAA Journal*, Vol. 30, No. 5, 1992, pp. 1228–1236.

[13]Giles, M. B., "Nonreflecting Boundary Conditions for Euler Equation Calculations," *AIAA Journal*, Vol. 28, No. 12, 1990, pp. 2050–2058.

[14]Buffum, D. H., and Fleeter, S., "The Aerodynamics of an Oscillating Cascade in a Compressible Flow Field," *Journal of Turbomachinery*, Vol. 112, No. 4, 1990, pp. 759–767.

[15]Hwang, C. J., and Wu, S. J., "Global and Local Remeshing Algorithms for Compressible Flows," *Journal of Computational Physics*, Vol. 102, No. 1, 1992, pp. 98–113.

[16]Smith, S. N., "Discrete Frequency Sound Generation in Axial Flow Turbomachines," Cambridge Univ. Rept. CUED/A-Turbo/TR 29, Cambridge, England, UK, 1971.

[17]Fleeter, S., "Fluctuating Lift and Moment Coefficients for Cascaded Airfoils in a Nonuniform Compressible Flow," *Journal of Aircraft*, Vol. 10, No. 2, 1973, pp. 93–98.

[18]Wolff, J. M., and Fleeter, S., "Single Passage Euler Analysis of Oscillating Cascade Unsteady Aerodynamics for Arbitrary Interblade Phase Angle," AIAA Paper 93-0389, Jan. 1993.

[19]Buffum, D. H., and Fleeter, S., "Wind Tunnel Effects in a Linear Oscillating Cascade," American Society of Mechanical Engineers Paper 91-GT-133, June 1991.